A. Romei, D. Vimercati, A.M.A. Guardone, G.B.A. Persico
Amplification of Operational Uncertainty Induced by Non-Ideal Flows in Supersonic Turbine Cascades
Journal of Engineering for Gas Turbines and Power, Vol. 142, N. 8, 2020, 081006 (15 pages)
doi:10.1115/1.4047770

Amplification of operational uncertainty induced by non-ideal flows in supersonic turbine cascades

Alessandro Romei[a,*], Davide Vimercati[b,c], Alberto Guardone[b], Giacomo Persico[a]

[a] *Department of Energy, Politecnico di Milano, Via Lambruschini 4, 20156 Milano, Italy*
[b] *Department of Aerospace Science and Technology, Politecnico di Milano, Via La Masa 34, 20156 Milano, Italy*
[c] *Institut für Thermodynamik, Universität der Bundeswehr München, 85577 Neubiberg, Germany*

Abstract

In high-temperature transcritical organic Rankine cycles (ORCs) the expansion process may take place in the neighbourhood of the thermodynamic critical point. In this region, many organic fluids feature a value of the fundamental derivative of gas dynamics Γ that is less than unity. As a consequence, severe non-ideal gas-dynamic effects may be possibly observed. Examples of these non-ideal effects are the non-monotonic variation of the Mach number along an isentropic expansion, oblique shocks featuring an increase of the Mach number and a significant dependence of the flow field on the upstream total state. To tackle this latter non-ideal effect, an uncertainty-quantification strategy combined with Reynolds-averaged flow simulations is devised to evaluate the turbine performance in presence of operational uncertainty. Results clearly indicate that a highly non-ideal expansion process leads to an amplification of the operational uncertainty. Specifically, given an uncertainty of $\approx 1\%$ in cycle nominal conditions, the mass flow rate and cascade losses vary $\pm 4\%$ and ± 0.75 percentage points, respectively. These variations are four and six times larger than those prompted by an ideal-like expansion process. The flow delivered to the first rotating cascade is severely altered as well, leading to local variations in the rotor incidence angle up to $10\,^\circ$. A decomposition of variance contributions reveals that the uncertainty in the upstream total temperature is mainly responsible for these variations. Finally, the understanding of the physical mechanism behind these changes allows us to generalise the present findings to other organic-fluid flows.

Keywords: non-ideal gas dynamics, uncertainty quantification, supersonic turbines, organic Rankine cycles

1. Introduction

The reduction of greenhouse gas emissions, along with the aim of a cleaner and more sustainable energy production, should be primarily pursued by exploiting a tailored high-efficient solution for the specific energy-conversion problem. In this perspective, organic Rankine cycle (ORC) power systems might represent the most efficient solution for a variety of applications, e.g. geothermal systems [1], small-scale solar-powered technologies [2], biomass-fired systems [3] and waste-heat recovery applica-

*Corresponding author
Email address: alessandro.romei@polimi.it (Alessandro Romei)

tions [4]. In an effort of raising the cycle efficiency, many modifications to the single-level saturated configuration were historically proposed. Among the various solutions, several studies outlined that a transcritical (or supercritical) cycle configuration may potentially be more efficient than its subcritical counterpart [5, 6].

One of the key factor in the determination of the cycle efficiency is a proper turbine design [7]. Due to the combination of high expansion ratio and low enthalpy drop, which couple with low values of the speed of sound, axial-turbine optimizations result in configurations made by a few supersonic or transonic blade rows [8, 9]. Furthermore, the first-stage nozzle cascade usually provides the largest pressure ratio, operating in highly supersonic flow regimes and delivering to the first rotating-blade row a highly non-uniform flow. The same flow features and connected fluid-dynamic challenges are shared with the supersonic stator of the centripetal (or radial-inflow) layout [10, 11]. For this reason, most of the research effort has focused on the design of the first supersonic stator [12, 13], as mainly responsible for the turbine efficiency degradation.

These flow features are even exacerbated when dealing with transcritical ORCs. As a matter of fact, the spread of transcritical configurations may be impeded by the challenge connected with the design of the turbine, whose expansion process occurs in the close proximity of the thermodynamic critical point, thereby featuring larger departures from the ideal-gas behaviour than the one found in the subcritical layout. A well-know parameter to quantify the volumetric deviation from the ideal-gas law is the compressibility factor $Z = Pv/RT$, where R is the specific gas constant. Besides, the evolution of the speed of sound along isentropic expansion can be fundamentally different for molecularly complex fluids when approaching the critical point from that observed in ideal flows. This discrepancy clearly emerges by inspecting the thermodynamic parameter Γ, defined as

$$\Gamma = 1 + \frac{\rho}{c}\left(\frac{\partial c}{\partial \rho}\right)_s, \tag{1}$$

which is called the fundamental derivative of gas dynamics [14]. In the above definition, ρ is density, s is the specific entropy and $c = (\partial P/\partial \rho)_s^{1/2}$ is the speed of sound, in which P is the pressure. If $\Gamma > 1$, the speed of sound decreases upon isentropic expansion; this is the typical behaviour of polytropic gases (i.e. ideal gases with constant specific heats) for which $\Gamma = (\gamma + 1)/2$, where $\gamma > 1$ is the ratio of the specific heats. On the contrary, the speed of sound increases following an isentropic expansion if $\Gamma < 1$. Thermodynamic states exhibiting $\Gamma < 1$ are found in the single-phase vapour region of many molecularly complex fluids for pressures and temperatures of the order of their critical-point values [15, 16, 17] and in the near-critical two-phase region of most substances [18]. Based on the peculiar speed-of-sound evolution when $\Gamma < 1$, which identifies the so-called *non-ideal gas-dynamic regime*, several non-ideal gas effects may arise, e.g. a non-monotonic variation of the Mach number along an isentropic expansion [19] and oblique shocks producing an increase of the Mach number [20]. On top of those, the expansion process reveals a significant sensitivity on the upstream total states, as experimentally demonstrated by Spinelli *et al.* [21].

A recent work conducted by the authors showed that non-ideal effects can also occur in turbomachinery flows, triggering unexpected operation with respect to the one encountered in ideal-gas flow applications [22]. Nonetheless, non-ideal effects are found only in a smaller domain of the entire non-ideal gas-dynamic regime. For an ideal gas with constant specific heats, $1 < \Gamma \leq 1.33$ and the well-known dilute gas behaviour is recovered in turbine flows. Such an ideal-like behaviour is also observed in the $\Gamma < 1$ region, provided that the Γ is close to unity. To account for this difference, a further distinction based on the value of Γ is made hereinafter: we classify the operating conditions as *ideal-like operating regime* whenever $0.8 \lesssim \Gamma < 1$ in the supersonic expansion, yielding a turbine aerodynamics quantitatively similar to its ideal-gas counterpart. On the other hand, $\Gamma \lesssim 0.8$ in the supersonic expansion identifies the *non-ideal operating regime*, whereby non-ideal effects may play a significant role in the cascade operation. Based on the results of this work, we anticipate that when $\Gamma \lesssim 0.8$ non-ideal effects commences increasingly affecting the cascade aerodynamics. Even so, it is worth to highlight that the threshold between the two operating regimes is not a well-defined boundary and further fundamental studies aiming at developing a comprehensive theory are still urgently needed. For convenience, we will refer to turbine cascades operating in the ideal-like and non-ideal operating regime as *ideal-like cascade* and *non-ideal cascade*, respectively. The same designations will be also used to distinguish the corresponding flow features.

This work follows up our previous discussion on non-ideal effects in turbomachinery [22]. Since non-ideal effects can only occur in specific thermodynamic conditions, whether operational uncertainty in the power cycle affects the turbine operation in a non-ideal gas-dynamic regime still deserves a proper answer. To this end, a comparative analysis between an ideal-like and a non-ideal supersonic nozzle cascade is performed by introducing uncertainties in the values of maximum temperature and pressure of the power cycle, as well as in the condensation temperature.

Cycle uncertainties are properly converted into first-stator operational uncertainty, enabling their formulation in computational fluid-dynamic (CFD) simulations in the form of variations in flow boundary conditions. A surrogate-based uncertainty-quantification analysis is combined with CFD simulations to propagate such operational uncertainty on the cascade aerodynamics. Similar procedures of uncertainty quantification were successfully applied to estimate ORC turbomachinery performance in what we called ideal-like conditions [23, 24]. In the present work, the methodology is applied to both ideal-like and non-ideal cascades, comparing their probabilistic performance in terms of cascade losses, alteration of the flow field delivered to the first rotor and implications on the corresponding power cycles. Since the underlying gas-dynamic physics is very different between the two cases, the subsequent impact of operational uncertainty is expected to differ as well.

The paper is structured as follows. In §2, we delineate the framework of this work via numerical examples of simplified expanding flows, introducing the problem of the operational-uncertainty amplification in non-ideal expansion processes. Next, we

outline the engineering problem in §3, consisting in ORC power cycles and corresponding turbines. The flow solver and the uncertainty-quantification strategy are detailed in §§3.1–3.2 , respectively. Firstly, we study the probabilistic performance of supersonic first-stage nozzle cascades, per se, in §4, then we analyse the implication on the subsequent rotating-blade rows in §5. Gathering the overall turbine results, we discuss the consequences of operational uncertainty from the power-cycle perspective in §6. Finally, although expansion processes focus on a specific organic fluid, in §7 we generalise our conclusion to a wider class of organic compounds by means of simplified quasi-one-dimensional flows. The new insight gained into turbines operating in non-ideal conditions allows us to draw recommendations for the control of future transcritical ORCs, making aware the cycle designer of the potential higher variability triggered by non-ideal operation.

2. Impact of operational uncertainty in quasi-one-dimensional expanding flows

We briefly describe archetypal examples of non-ideal expanding flows with a steady quasi-one-dimensional approach [25], which assumes an inviscid and constant total-enthalpy flow through a variable duct area. This simplified flow description allows us to illustrate how operational uncertainty couples with non-ideal gas dynamics, mirroring the thermodynamic conditions and the expansion processes that will be discussed later in the supersonic turbines. In this section, we limit our analysis to the linear siloxane MM (hexamethyldisiloxane, $C_6H_{18}OSi_2$), whose thermodynamic properties are computed with the multi-parameter equation of state detailed in Thol *et al.* [26], because it may show significant non-ideal effects besides being a popular working fluid in high-temperature ORC applications [6]. In the last section §7, we will generalise the concept here described to other classes of organic fluids (e.g. refrigerants, hydrocarbons) commonly employed in the ORC field.

With reference to the classification made in the introductory section, we consider an ideal-like expanding flow, i.e. $\Gamma \gtrsim 0.8$ in the supersonic expansion, with upstream total conditions $P^t = 8\,\mathrm{bar}$ and $T^t = 272.5\,^\circ\mathrm{C}$, where P^t and T^t are the total pressure and total temperature, respectively, and a non-ideal expanding flow, i.e. $\Gamma \lesssim 0.8$ in the supersonic expansion, with upstream total conditions $P^t = 40\,\mathrm{bar}$ and $T^t = 272.5\,^\circ\mathrm{C}$. The upstream total conditions can vary up to $\pm 1.25\%$ with respect to their design values (temperature measured in Celsius degree), obeying to independent uniform distributions. Figure 1 reports the distribution of the design area ratio A/A^* with the outlet pressure P, where A^* is the sonic throat, along with 200 random realizations. The area ratio A/A^* has a direct engineering implication because it is connected with the design of the diverging portion of a nozzle aimed at producing a smooth shock-free expansion process (adapted expansion) for a given outlet pressure. To illustrate the role of an uncertainty in the total conditions on the two expansion processes, we choose a specific area-ratio value, namely $A/A^* = 2.4$, as representative of a manufactured nozzle (or a conceptually equivalent supersonic stator) operating under total-condition uncer-

tainty. The introduction of operational uncertainty barely affects the ideal-like expansion process (variations lower than 0.5% on the exit pressure), see Fig. 1(a), while it has a great impact on the non-ideal one (the adapted outlet pressure varies from -11% to $+6\%$ with respect to the design value), see Fig. 1(b). In this latter case, assuming that the area ratio was chosen to deliver the design pressure ratio, the variation observed in the outlet pressure imposes to the flow either a recompression via shocks, when the outlet pressure is lower than the design one, or a post-expansion via rarefaction fans, when the outlet pressure is higher than the design one.

The same behaviour is qualitatively expected in turbomachinery flows when operating in similar non-ideal conditions. The flow-structure modifications (from an adapted expansion to compression shocks and rarefaction fans) induced by the amplification of operational uncertainty through the expansion process with $\Gamma \ll 1$ will arguably affect the turbine performance, triggering significant off-design operation with a subsequent departure from the nominal efficiency. To anticipate future transcritical ORC shortcomings, a quantitative estimate of this mechanism of turbine efficiency degradation becomes crucial, motivating the rationale of the present work.

3. Problem contextualisation and definition

Representative subcritical and transcritical ORC configurations are identified as references for the following analyses. Their constitutive thermodynamic transformations are reported in the well-known T–s (temperature–entropy) diagram in Fig. 2. These cycle layouts were inspired by the combined heat and power application detailed in Colonna *et al.* [27], which made use of the siloxane MDM (octamethyltrisiloxane, $C_8H_{24}O_2Si_3$) as working fluid. In spite of the higher saturation pressure at the condensation temperature, the siloxane MM is considered here because it may exhibit non-ideal gas-dynamic effects for temperature levels below its thermal-stability limit [28, 29] and consistently with the maximum temperature prescribed by the application. In addition, both siloxanes are currently employed in combined heat and power applications [7], thus preserving the technical relevance of following outcomes regardless of the specific fluid selection. The maximum temperature is set to $T_{max} = 272.5\,^{\circ}\mathrm{C}$ and it is kept equal for both cycles. For the subcritical cycle, we prescribe the same maximum pressure of the original configuration, i.e. $P_{max} = 8\,\mathrm{bar}$ [27]. On the other hand, the choice of the maximum pressure for the supercritical layout ($P_{max} = 40\,\mathrm{bar}$) offers the opportunity to achieve low values of Γ along the expansion process while retaining a conservative margin from the two-phase region. The outlet turbine pressure, corresponding to saturated condition at the condensation temperature ($T_{cond} = 85\,^{\circ}\mathrm{C}$), is set to 0.63 bar for both cycles.

As outlined in the §2, the blade cascade that most suffer from operational uncertainty is the first stator, which features a supersonic flow regime and the largest departure from the ideal-gas behaviour, as illustrated in Fig. 3, where both Z and Γ isocurves are reported. To analyse the first-stator performance via accurate CFD simulations, proper boundary conditions must be assigned. The maxi-

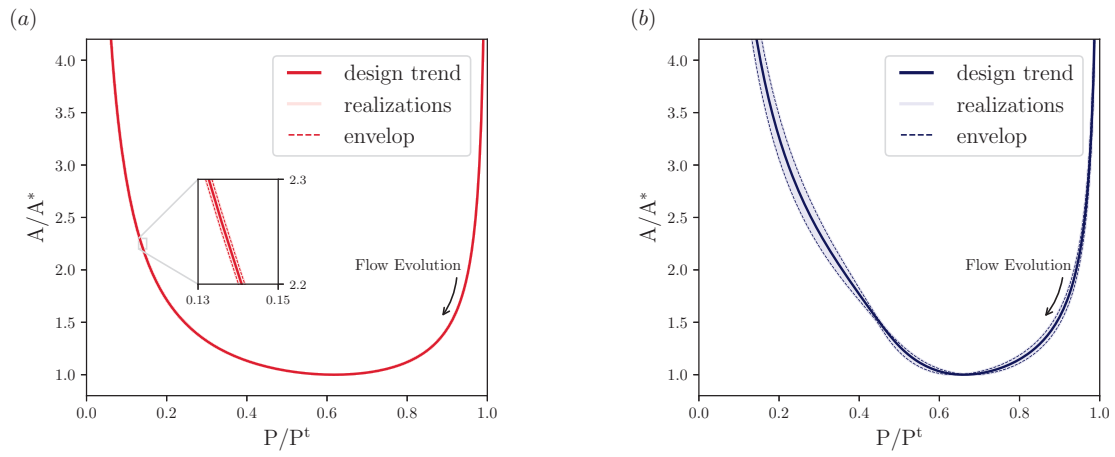

Figure 1: Design area-ratio distributions predicted by the quasi-one-dimensional theory for an ideal-like expanding flow (with total states $P^t = 8\,\text{bar}$ and $T^t = 272.5\,°\text{C}$) and a non-ideal expanding flow (with total states $P^t = 40\,\text{bar}$ and $T^t = 272.5\,°\text{C}$) of fluid MM, along with 200 independent uniformly distributed realizations assuming ±1.25% uncertainty in both the design total pressure and temperature.

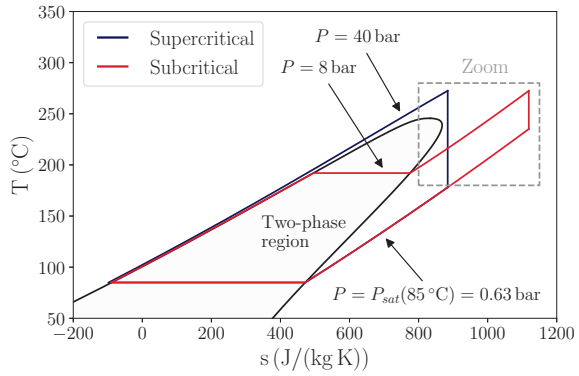

Figure 2: Representative subcritical and transcritical organic Rankine cycles with MM as working fluid.

mum pressure and temperature of the power cycles can be directly prescribed as inlet boundary conditions. The pressure condition at the stator outlet, given the overall expansion ratio dictated by the cycle, depends on the number of stages arranged in the machine and their specific reaction degrees. The enthalpy drops are distributed among cascades with the following rationale [30]: the first stage provides the highest enthalpy drop ($\chi \leq 0.25$, where $\chi = \Delta h^R_{is}/\Delta h^{st}_{is}$ is the isentropic reaction degree and Δh^R_{is}, Δh^{st}_{is} are the isentropic enthalpy drop across the rotor and the stage, respectively), while the remaining stages operate at the maximum efficiency point ($\chi \approx 0.5$). As far as the number of stages is concerned, on the one hand, we select a single-stage axial turbine for the subcritical cycle, resulting in a outlet first-stator pressure of $P_1 = 1.07\,\text{bar}$ with a minimum $0.9 < \Gamma < 1.0$ in the supersonic expansion. The stator expansion ratio ($\beta = P^t_0/P_1 = 7.5$) agrees with previous studies of similar ORC supersonic cascade in ideal-like conditions [27, 12]. On the other hand, a five-stage axial turbine is chosen for the transcritical cycle, providing a pressure of $P_1 = 12.5\,\text{bar}$ at the exit of the first stator. Along the isentropic supersonic expansion, the minimum value of Γ is found in the range $0.3 < \Gamma < 0.4$, revealing the non-ideal character of the expansion. For the non-

ideal case, a higher number of stages was dictated by an overall lower value of the speed of sound close to the thermodynamic critical point, which lead to a highly supersonic Mach number for comparatively lower pressure ratios. As a further confirmation, based on quasi-one-dimensional calculations, the first-stator expansion ratio ($\beta = 3.2$) delivers a maximum Mach number $M \approx 1.8$, forcing the choice of converging-diverging profiles to efficiently accomplish the supersonic expansion. Besides, a five-stage axial configuration was recently proposed by one of the leading manufacturers in the ORC field [31]. The resulting upstream total conditions and the first-stator expansion processes are reported in Figure 3 for the two cases.

Pressure, Mach number and total-pressure fields for the ideal-like and non-ideal cascade at design conditions are reported in Fig. 4(a)-(b), respectively. These results are obtained with the numerical settings detailed in §3.1 and imposing the boundary conditions derived previously in this section. Because of the prescribed flow turning is similar for the two conditions ($\Delta\alpha \approx 77°$, where α indicates the absolute flow angle measured from the meridional direction), the two cascades share the same solidity $c_{ax}/s = 0.74$, where $c_{ax} = 0.33\,\mathrm{m}$ is the blade axial chord and s is the blade pitch. The blade profiles for the two cases are designed using our in-house surrogate-based shape-optimisation tool FORMA [13], which adapts the blade profile to the corresponding expansion process, thus enabling relatively smooth expansions through the blade channels.

As a result of the blade optimisation, the entropy production across fish-tail shocks, arising

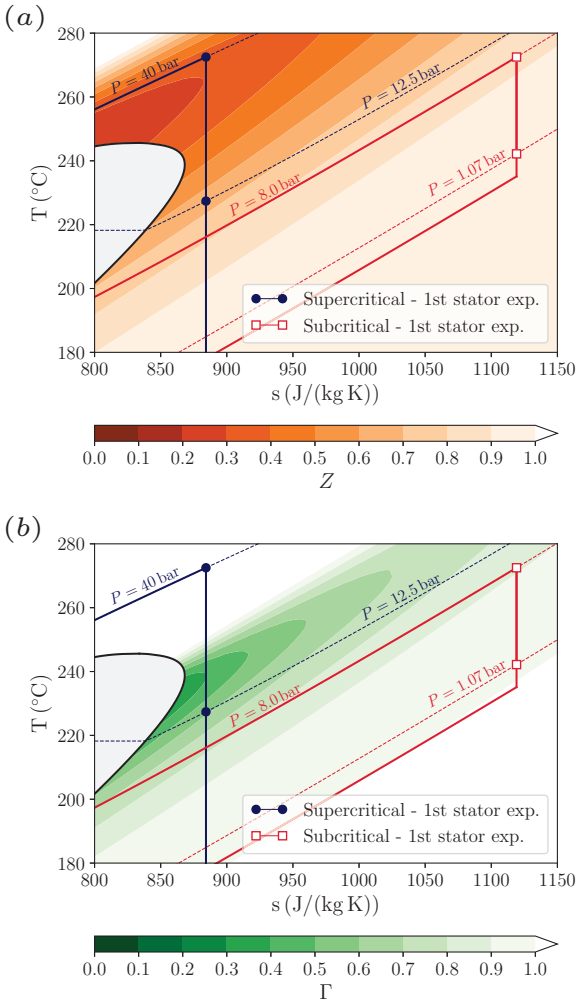

Figure 3: Zoom of Figure 2, highlighting first-stator expansion processes. A map of the compressibility factor Z and fundamental derivative of gas dynamics Γ are superposed in frames (a) and (b), respectively.

from the flow turning around the finite-thickness trailing edge, is only a small share of the overall entropy produced by the cascade. The larger contribution to cascade losses is provided by viscous effects in the wake development and subsequent mixing process downstream of the cascade. In this regard, in agreement with other works, a comparison between the two total-pressure fields reveals a

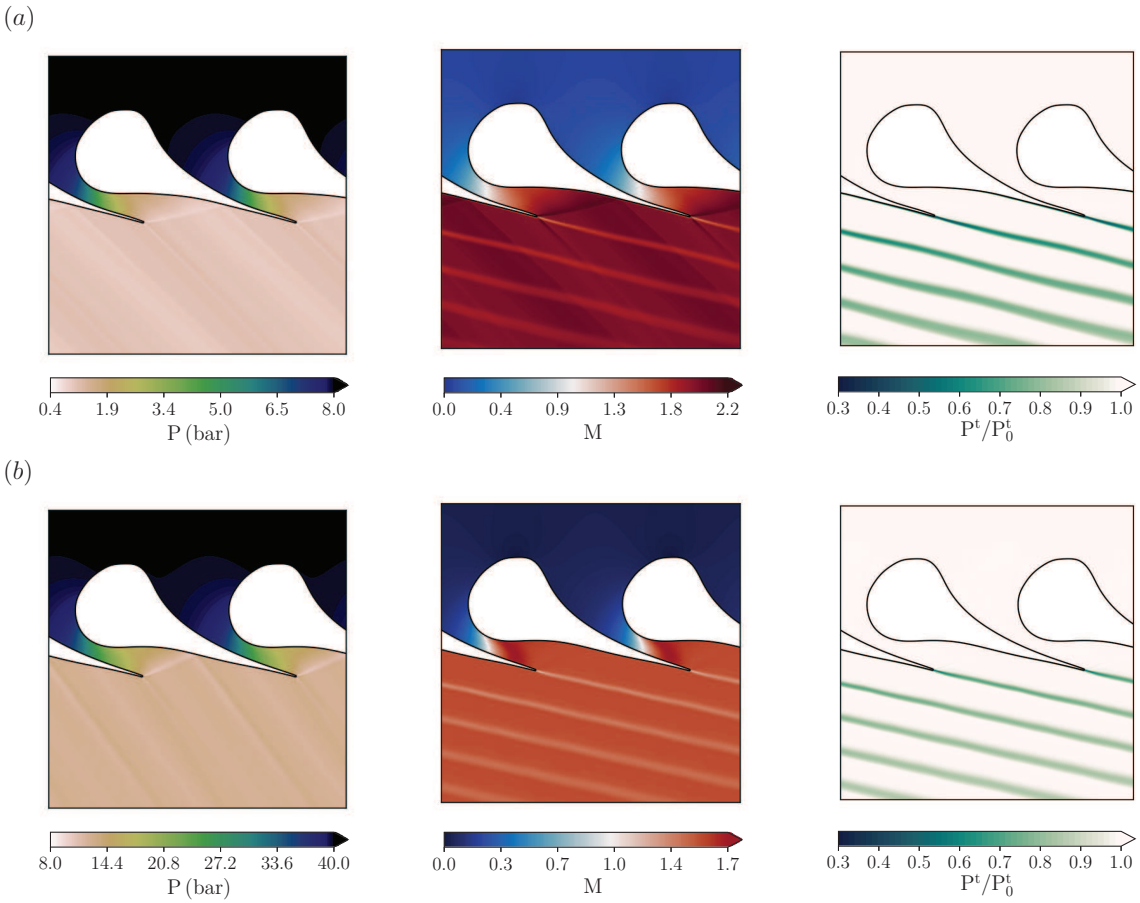

Figure 4: Pressure, Mach number and normalised total-pressure fields for the nozzle cascades operating in the ideal-like (a) and non-ideal (b) operating regimes at nominal conditions.

wider wake for the ideal-like scenario [32, 33]. The most accredited explanation is that a higher value of the Prandtl-Meyer function, characterising non-ideal flows $\Gamma \ll 1$, induces higher turning angles, thus a reduced separation region behind the trailing edge. Overall, no substantial differences are found in the entropy-production mechanisms between the ideal-like and non-ideal cascade.

Upon inspection of the Mach number field in Fig. 4(b), a non-monotonic variation of the Mach number is observed, with the local minimum of the Mach number located at the blade outlet. This follows immediately from the analysis of Cramer & Best [19], in which the parameter

$$J = \frac{\rho}{M}\frac{dM}{d\rho} = 1 - \Gamma - \frac{1}{M^2} \qquad (2)$$

is introduced as a non-dimensional measure of the Mach number derivative with the density. The condition $J > 0$ is a necessary condition to have a Mach number that decreases along isentropic expansions. A possible advantage deriving from this condition is the enhanced uniformity of the Mach number distribution within the stator-rotor axial gap, due to its reduced sensitivity to perturbations in the pressure field [22].

Finally, the definition of operational uncertainty has to be addressed. To the authors' best knowledge, the data reported in Zanellato *et al.* [34] is the only source of operational variability in running ORC power plants that is available in the open literature. Specifically, field measurements of temperature and pressure at the outlet of the evaporator (T_{eva}, P_{eva}) and temperature in the condenser (T_{cond}) are there reported for two-level saturated cycles. Although system layouts and working fluids are considerably different from the ones employed in this work, a similar variability in controlling an ORC power plant can be expected. Based on the published data, the following relative variations from nominal and/or average conditions are derived: $\Delta T_{eva}/T_{eva} \approx 1.25\%$, $\Delta P_{eva}/P_{eva} \approx 1.25\%$, $\Delta T_{cond}/T_{cond} \approx 1\%$ with temperatures expressed in degrees Celsius. Whilst outlet evaporator pressure and temperature can be directly prescribed as boundary conditions at the inlet of the turbine, the uncertainty in the condensation temperature must be propagated to the first-stator outlet pressure. Given $\Delta T_{cond}/T_{cond} \approx 1\%$, a sampling strategy is applied to derive the corresponding variations in first-stator outlet pressures $\Delta P_1/P_1$. Preliminary calculations assuming different stochastic scenarios [35] show that no qualitative differences emerge neither in the ideal-like nor in the non-ideal case when changing input distributions. Gathering all these information, operational uncertainties in first-stage nozzle cascades are formulated to be independently distributed as in Tab. 1.

3.1. Computational flow model

Computational fluid-dynamic simulations are performed with ANSYS–CFX 18.1®. Total pressure P_0^t and temperature T_0^t are set as inlet boundary conditions, along with a purely axial-flow direction. At the outlet, an average static pressure P_1 is imposed, accepting local pressure differences of 5%. The outlet domain is placed approximately at eight axial chords downstream of the trailing edge to avoid spurious pressure-wave reflections. Since only blade-to-blade effects are of interest, quasi-three-dimensional simulations are carried out by considering a straight stream tube around the midspan and by imposing a free-slip boundary condition at the hub and shroud. Finally, no-slip and adiabatic boundary condition are set to the blade wall, which is modelled as a smooth surface.

The Reynolds-averaged Navier-Stokes (RANS) equations are complemented with the $k-\omega$ SST turbulence model, whose inlet boundary conditions are set as turbulence intensity equal to 5% and eddy-to-molecular viscosity ratio equal to 10. The cascade Reynolds number, based on the mass-flow-averaged kinematic viscosity and velocity, evaluated both at the blade inlet and outlet, and on the blade chord, is high enough ($Re = 10^6 - 10^8$) to assume fully turbulent flow in all simulations. High-resolution schemes are employed in the discretisation of both flow and turbulence equations.

The multi-parameter equation of state expressed in terms of Helmholtz fundamental relations [26] is selected to compute the equilibrium thermodynamic properties of the siloxane MM. To speed-up the computation, a look-up-table approach is

Uncertainty		Ideal-like	Non-ideal
T_0^t (°C)	$\sim$	$\mathcal{N}(\mu = 272.5, \sigma = 1.175)$	$\mathcal{N}(\mu = 272.5, \sigma = 1.175)$
P_0^t (bar)	$\sim$	$\mathcal{B}(\alpha = 2, \beta = 4.5)$ on $[7.9, 8.1]$	$\mathcal{B}(\alpha = 2, \beta = 4.5)$ on $[39.5, 40.5]$
P_1 (bar)	$\sim$	$\mathcal{N}(\mu = 1.075, \sigma = 0.007)$	$\mathcal{N}(\mu = 12.5, \sigma = 0.024)$

Table 1: Summary of uncertainties accounted in this work along with their probabilistic distributions ($\mathcal{B}$: beta distribution; $\mathcal{N}$: normal distribution, μ, σ: mean and standard deviation of the normal distribution, α, β: shape parameters of the beta distribution).

adopted by making use of the NIST–REFPROP® database [36] in the generation of the thermodynamic tables. The table ranges are taken large enough to avoid any clips or extrapolations during the convergence process, with an accuracy of approximately 0.01 K and 0.05 bar for temperature and pressure, respectively.

Computations are performed on structured hexahedral meshes, where a proper cell clustering near blade walls is provided to ensure $y^+ \lesssim 1$, thus avoiding the introduction of wall functions in the solution. The grid-convergence assessment in terms of cascade loss coefficient $Y = (P_0^t - P_{2c_{ax}}^t)/(P_0^t - P_{2c_{ax}})$ (where the subscript $2c_{ax}$ indicates the section placed 2 axial chord downstream of the trailing edge) is reported in Fig. 5(a) for the two cascade configurations at the corresponding design conditions. The grid size with 200k elements in the blade-to-blade plane is selected hereinafter for both cases, accepting in the computation of the cascade loss coefficient a difference with respect to the finest value of less than 0.2 percentage points (pp).

3.2. Surrogate-based uncertainty quantification strategy

To derive statistically relevant information about turbine operation, one should sample from the input probability distributions a large number of boundary conditions, say $\mathcal{O}(10^6 - 10^8)$, and process each of them via CFD simulations to compute several realizations of the cascade performance. However, this methodology cannot be applied as it is because of the high computational cost required by the single CFD evaluation. To circumvent this problem, a surrogate-based strategy is devised. First, a smaller number of CFD cases is run to build a surface response of selected quantities that are indicative of the nozzle-cascade performance. Then, the surface response is used as a surrogate of the flow solver to process the large number of evaluations needed to derive statistically-relevant indications. In this work, polynomial-chaos (PC) representations [37] are used as surrogates of the flow model with respect to three operational parameters, namely T_0^t, P_0^t and P_1. Distinct PC expansions are computed for each output response, e.g. the cascade loss coefficient Y, the mass flow rate $\dot{m}$ processed by the cascade, besides others. The PC representation permits to express an output ran-

dom variable in a series of polynomials ψ mutually orthogonal to the probability measure ρ associated with the input uncertainties. For standard probability measures, a convenient choice is to select ψ in according to the Askey scheme [38], resulting in the Hermite and Jacobi polynomials for the normal and beta distributions assumed in this work, respectively. The implemented surrogate model, expressed in terms of cascade loss coefficient for illustrative purposes, can be then summarised by the following expression:

$$Y(T_0^t, P_0^t, P_1) = \sum_{i=0}^{p}\sum_{j=0}^{p}\sum_{k=0}^{p} \beta_{ijk}\psi_i(T_0^t)\psi_j(P_0^t)\psi_k(P_1)$$
$$\beta_{ijk} = \frac{1}{\langle \psi_i\psi_j\psi_k, \psi_i\psi_j\psi_k\rangle}\int_{\Xi} Y\,\psi_i\psi_j\psi_k d\rho_i d\rho_j d\rho_k \tag{3}$$

where, for the ease of readability, in Eq. (3) i, j, k indicate both the polynomial order p and the uncertainties which polynomials and probability measures refer to. The operator $\langle\cdot,\cdot\rangle$ expresses the inner product in the space $L^2(\Xi, \rho)$, where Ξ is the support of the probability density $\rho = \rho(T_0^t)\rho(P_0^t)\rho(P_1)$, see Tab. 1. The integrals to determine the PC coefficients β_{ijk} are solved by tensorization of the corresponding Gaussian quadrature rule of order q in each stochastic dimension, resulting in overall q^3 CFD evaluations. It is worth to recall that the numerical strategy integrates exactly all polynomials of orders up to $2q-1$. It follows that to integrate exactly Y, modelled of order q, the order of polynomials in the PC expansions ψ has to be truncated at $p = q - 1$. Once the PC representation is settled, statistics are computed by sampling the surrogate model, which can be effectively interrogated many times at almost-free computational cost. A pointwise PC expansion is used when processing trends and flow fields. Three quadrature orders are investigated in Fig. 5(b) in terms of cascade-loss distributions for the non-ideal case, which ought to represent the toughest stochastic problem in light of the expected larger variability. All quadrature orders produce very similar Gaussian distributions, whose minor differences are attributable to the sampling error. The difference in mean estimates is 0.002 pp between the PC representation built with $q = 4$ and $q = 5$. Since the same quadrature order is also preserved for other output variables, a conservative $q = 4$ is employed to produce all the following results. A complete uncertainty-quantification study consisting in 64 CFD runs required approximately 16 h on an Intel® Xeon® CPU E5-2630 v3 @ 2.40GHz equipped with 16 cores. One advantage of resorting to a PC representation over other surrogate methods is that the polynomial coefficients β_{ijk} can be directly used to estimate the total Sobol indices S^T, which quantify the global contribution of each uncertainty to the total variance of the quantity of interest [39].

4. Probabilistic performance of supersonic nozzle cascades

In this section, we outline the effect of operational uncertainties on the stator aerodynamics. From an integral perspective, the most significant indicator is the cascade-loss coefficient (following the definition provided in §3.1) and the processed mass flow rate. This latter quantity is particularly relevant because it directly establishes the

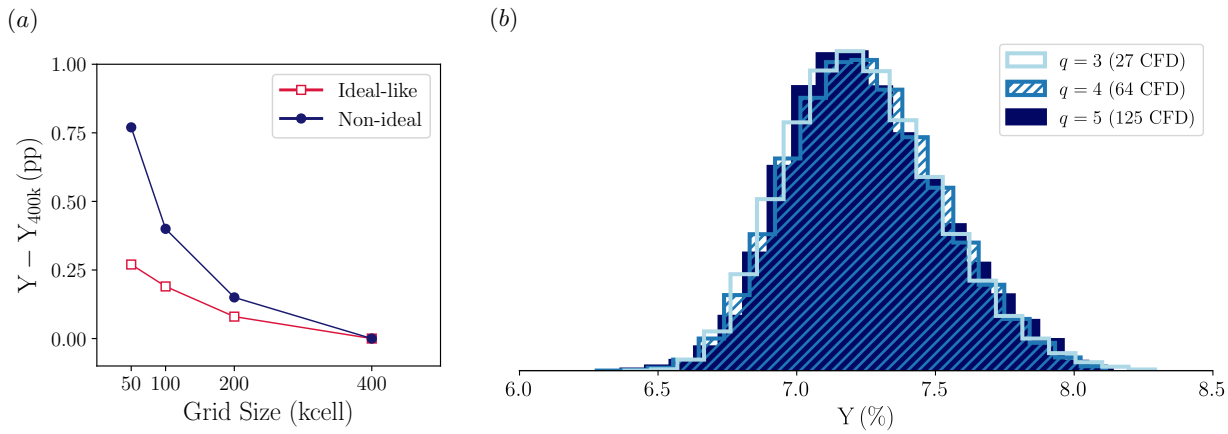

Figure 5: Computational tool verification in terms of (a) grid convergence for CFD calculations and (b) statistic convergence for PC representations. The grid size indicates the number of cells in the blade-to-blade plane. The statistic convergence is assessed on the non-ideal stochastic problem.

mass flow rate within the power cycle if the supersonic cascade is choked (as it usually occurs for converging-diverging blade profiles). To this end, the joint probability distributions in terms of normalised mass flow rate (with respect to the nominal value) and loss coefficient are reported in Fig. 6 for the two cascades. At first glance, substantial differences between the ideal-like (Fig. 6(a)) and non-ideal (Fig. 6(b)) cascade operation can be appreciated from both a quantitative and qualitative perspective. On a quantitative ground, the non-ideal loss distribution is characterised by a nearly symmetrical support that amount 1.5 pp (measured as a difference between the maximum and minimum value), which is six times larger than its ideal-like counterpart. Besides, the mass-flow-rate support is four times larger as well. On the other hand, an inspection of the joint-distribution shapes unveils different kinds of correlation between the two observed quantities, suggesting peculiar gas-dynamic evolutions under uncertainties. In particular, a significant negative dependence correlates the mass flow rate and loss coefficient for the non-ideal case. Instead, the joint distribution does not suggest any clear correlations between variables in the ideal-like scenario.

A classification of the importance of the operational uncertainty on the cascade performance can help to understand these fundamental differences. Figure 7 reports a sensitivity analysis based on total Sobol indices S^T, which quantifies the contribution of each uncertainty (i.e. T_0^t, P_0^t and P_1) to the total variance of mass flow rate in Fig. 7(a) and cascade losses in Fig. 7(b).

For what concerns the mass flow rate, the resulting zero contribution of the downstream pressure indicates that both supersonic cascades are choked. Nonetheless, the predominant variable contributing to the mass-flow-rate uncertainty varies between the two cases. For the ideal-like regime, the total pressure overcomes the contribution of the total temperature, while roles are reversed in the non-

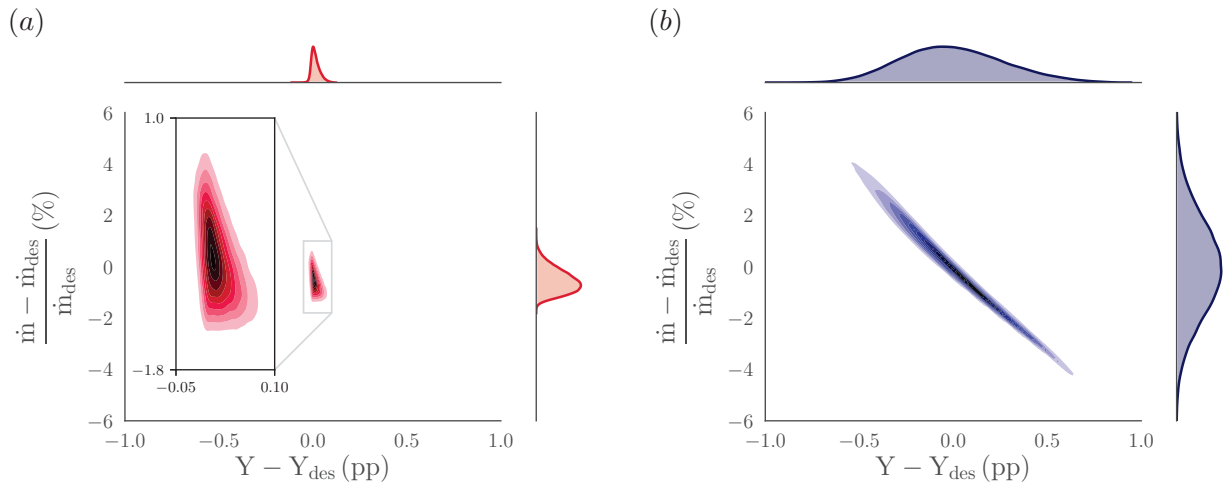

Figure 6: Joint probability distributions for the normalised mass flow rate and cascade-loss coefficient in the ideal-like (a) and non-ideal (b) operating regime.

ideal regime. Recalling that the mass flow rate under choked operation exclusively depends on the thermodynamic properties at the throat section, indicated with superscript * hereinafter, via the relationship $\dot{m} = \rho^* c^* A^*$, where the throat area A^* is geometrically fixed, a variation in the upstream total state defines different isentropes along with the expansion in the converging part occurs. In ideal-like operation, the total pressure has a larger influence on the density while the speed of sound is more sensitive to variations in the total temperature. To support this last statement, a parametric study imposing a separate increase in the total pressure and total temperature is considered under the assumptions of the quasi-one-dimensional approach described in §2. The magnitude of these increases mirrors the maximum variations imposed in the stochastic analysis, i.e. +1.25% of the corresponding total variables. A resulting increase of 0.1 bar in the nominal total pressure affects more the density value ($\Delta\rho^*/\rho^*_{des} = +1.4\%$) than a separate increase of 3.5 °C in the nominal total temperature ($\Delta\rho^*/\rho^*_{des} = -1.0\%$). Furthermore, an opposite but comparable-in-magnitude variation in the speed of sound ($\Delta c^*/c^*_{des} = +0.6\%$) is prompted by the total temperature rise, while a significant lower sensitivity is found against the total-pressure increase ($\Delta c^*/c^*_{des} = -0.1\%$). Since the mass flow rate is ultimately provided by the product $\rho^* c^*$, the total-pressure contribution overall prevails over the total temperature as reported in Fig. 7(a). Nonetheless, the smooth variations of density and speed of sound along ideal-like isentropes leads to a quantitatively small departure from the mass-flow-rate nominal value, as evidenced in the corresponding distribution of Fig. 6(a).

An analogous parametric study is conducted for the non-ideal case, where similar relative increases with respect to the upstream total variables are applied, resulting in 0.5 bar and 3.5 °C for the total pressure and total temperature, respectively. The total temperature rise at fixed

total pressure provides a variation in the density and speed of sound equal to $\Delta\rho^*/\rho^*_{des} = -4.5\%$ and $\Delta c^*/c^*_{des} = -0.8\%$, respectively. The opposite, i.e. an increase in total pressure at fixed total temperature, produces $\Delta\rho^*/\rho^*_{des} = +0.8\%$ and $\Delta c^*/c^*_{des} = +1.1\%$. These quantitative variations explains why and how total temperature mostly contributes to the mass-flow-rate uncertainty.

Analogous physical considerations based on loss-variance decomposition, see Fig. 7(b), can explain the differences observed in the loss distributions of Fig. 6. The underlying expansion process, to which the cascade aerodynamics is strictly correlated, depends on both the prescribed expansion ratio, given by the combination of upstream and downstream pressure, and on its evolution with respect to the upstream total quantities, as explained in §2 for simplified expanding flows. In the limit of polytropic-gas flows, the expansion ratio uniquely determines the expansion evolution. This behaviour is partially recovered in the ideal-like cascade, where the expansion process is almost entirely determined by the expansion ratio, as highlighted in Fig. 7(b) by the higher contributions of the pressure upstream and downstream of the cascade. If the expansion ratio varies, the flow must adjust downstream of the blade opening to match the prescribed expansion process, resulting in a different oblique-shock/post-expansion pattern at the trailing edge and a subsequent variation of aerodynamic losses. A non-negligible contribution of the total temperature copes with the small degree of non ideality characterising ideal-like operation ($\Gamma \gtrsim 0.8$), as further evidenced by the corresponding simplified flow in §2, where a small yet non-zero variation in the expansion evolution is observed when total quantities are changed.

On the contrary, non-ideal cascade losses are completely dominated by a variation in the upstream total temperature, which overcomes the contribution given by a variation in the expansion ratio, either in terms of upstream total pressure or downstream static pressure. As a matter of fact, the adapted expansion process, which can be conveniently represented by A/A^*, exhibits a significant sensitivity to total-temperature variations [22]. Therefore, as a result of a change in the total temperature, the desired area ratio to have a shock-free expansion process changes while the area ratio across the cascade is geometrically imposed, thus inducing off-design conditions that are more severe than the ones that are triggered by a change in the pressure ratio.

Finally, the hierarchy of operational uncertainties established from the variance decomposition also clarifies the shape morphology of the joint distributions found in Fig. 6. For the non-ideal case, the prevailing uncertainty is the total temperature for both the cascade loss and mass flow rate, acting in an opposite sense (e.g. whenever the total temperature increases, the mass flow rate decreases while the cascade loss increases). Alongside a reduction of mass flow rate as described in the parametric study conducted before in this section, an increase in the total temperature leads to a decrease of A/A^* at a given outlet pressure. Therefore, when A/A^* becomes lower than the design one, the cascade is expanding more than the requested in the blade channel, then forcing the flow to adjust itself at the trailing edge via compression shocks to match the

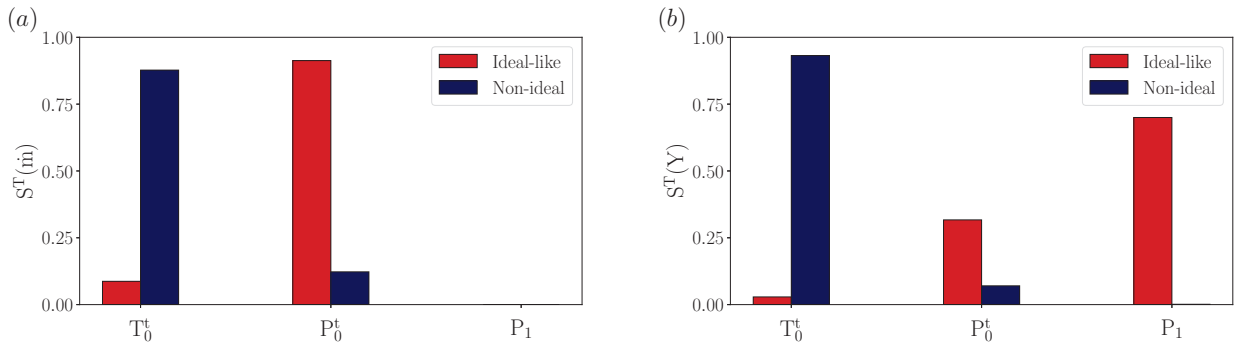

Figure 7: Total Sobol indices of (a) mass flow rate and (b) cascade loss for the ideal-like and non-ideal operating regime.

prescribed outlet pressure with a consequent rise in the aerodynamic losses. The deviation from a limiting linear joint distribution is given by the smaller effect provided by the total pressure to both the mass flow and losses. The absence of a key uncertainty shared by both quantities in the ideal-like operating regime conceals the underlying structure of the corresponding joint distribution.

So far, the analysis focuses on integral parameters which are explanatory of the cascade aerodynamics. Nevertheless, such large performance variations should be followed by as many changes in the local flow field. To this end, we compute the coefficient of variation, $CoV = \sigma/\mu$, where σ and μ represent the standard deviation and the mean, respectively, of pressure, Mach number and total pressure fields in Fig. 8. It is worth to underline that a stochastic field does not have a physical meaning, per se, i.e. there is not a proportional relationship between a peak in the CoV and the actual value of the corresponding quantity.

As expected, ideal-like and non-ideal fields exhibit significant dissimilarities. In supersonic turbines, the supersonic flows from the pressure and suction side meet at the trailing edge. In turning around the trailing edge to a shared direction, they first expand via rarefaction fans and, subsequently, they possibly generate shock waves which will propagate into the flow field. As evidenced by Fig. 4, for both nominal cases only the flow coming from the pressure side generates a shock to accomplish the turning process. This shock reflects on the suction surface of the adjacent blade, interacting with the suction-side boundary layer, running downstream of the cascade afterwards.

Operational uncertainty in the ideal-like case will only affect the intensity of the shock reflection and the subsequent interaction with the adjacent-blade suction side, without considerably modifying the shock strength that stems from the the pressure side (pressure values across the shock are unaltered). This behaviour can be again explained by referring to A/A^*. In ideal-like conditions, A/A^* is almost constant under operational uncertainty, hence the expansion process in the blade channel remains unaltered, not affecting the shock pattern at the blade opening. On top of that, the outlet pressure is also varied, imposing a flow adjustment downstream of the blade opening, i.e. in the shock reflection, to match the prescribed boundary con-

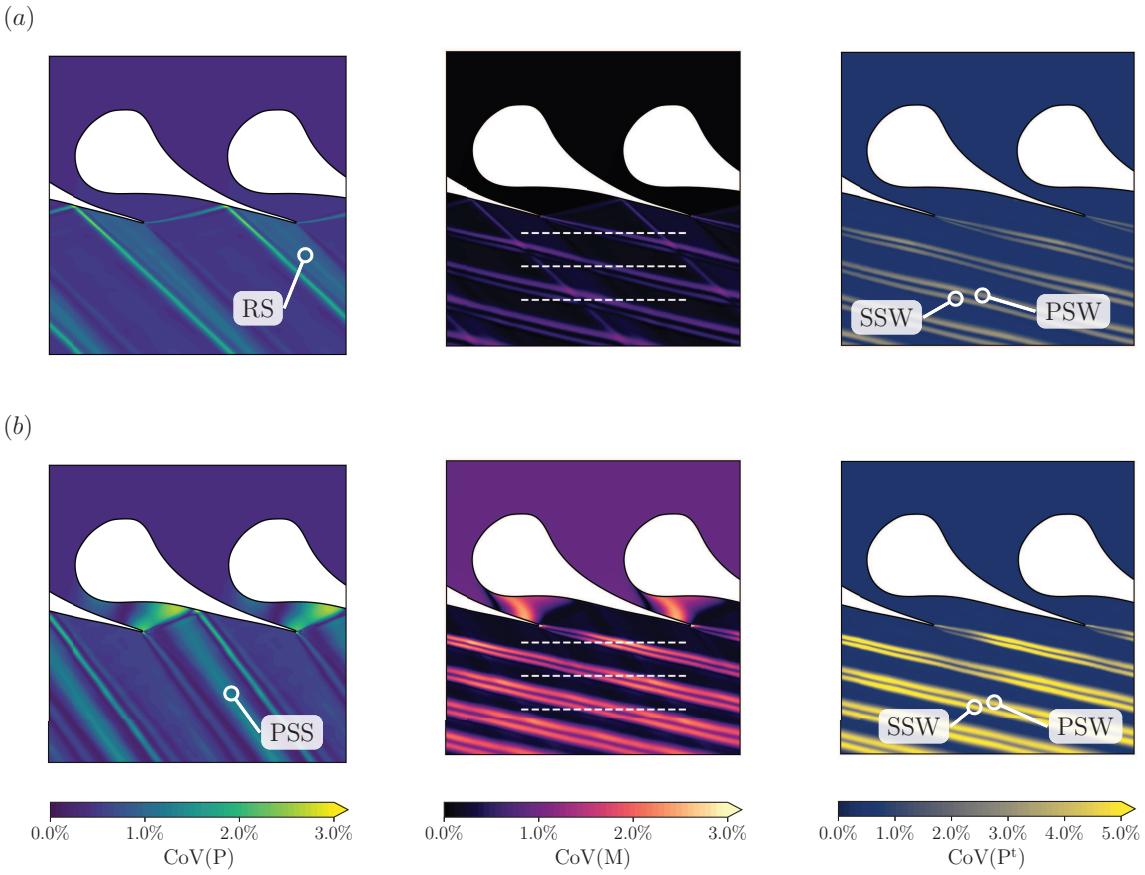

Figure 8: Pressure (P), Mach number (M) and total pressure (P^t) coefficient-of-variation (CoV) fields for the ideal-like (a) and non-ideal (b) cascade. RS indicates the peak of variation induced by a reflected-shock intensity change, while PSS refers to the uncertainty induced by a modification in the pressure-side shock strength. PSW and SSW highlight the uncertainty in the pressure-side and suction-side branch of the wake, respectively. The white dashed lines indicate three axial traverses at $x/c_{ax} = 1.15, 1.45, 1.75$, where pitchwise distributions are extracted..

dition. Indeed, given a nearly constant pressure value upstream of the reflected shocks, the highly uncertain value of the pressure downstream, as illustrated by the marker RS in Fig. 8(a), is a clear indication of the shock-strength change. The periodicity is restored by a subsequent variation in the shock pattern at the trailing edge on the suction side, i.e. given a lower/higher value of pressure as a consequence of the reflected-shock modification, the flow will turn less/more accordingly. A variation in the trailing-edge shock pattern will also affect the wake formation and evolution. In this regard, two distinct effects combines in the generation of the wake: (i) a variation in the turning process, strictly connected with the shock-strength modification, will induce a different wake width, and (ii) a variation in the pressure-gradient downstream of the cascade will produce a change in the outlet flow angle [40]. As a result, a bulk of an unaltered wake splits into two peaks of uncertainty (named PSW

and *SSW* in Fig. 8), which includes both the direction and width change. The wake changes in depth (i.e. minimum total pressure) as well, due to the base-pressure variation to comply with the prescribed turning process, thus altering the nominal cascade losses [41] as quantitatively discussed in the first part of the section.

On the other hand, a predominant uncertainty in the trailing-edge shock strength on the pressure side emerges from the analysis of non-ideal stochastic fields in Fig. 8(b). By virtue of the aforementioned variations in A/A^*, it is not surprising that the shock at the cascade opening is the flow structure most affected by uncertainties. As long as the geometrical ratio is fixed, the variation in A/A^* triggered by a non-ideal gas dynamics can impose a smaller or larger recompression than the one in design conditions. For example, let us assume that A/A^* reduces compared to the design value, which in turn fixes the geometrical ratio. Then, the larger diverging area imposed by the geometry force the flow to expand more in the blade channel, requiring a stronger recompression via shock at the blade opening to match the outlet boundary condition. Although the highest variation is found upstream of the shock, a noteworthy pressure field variation is also found downstream of the shock, marked as *PSS* in Fig. 8(b), which will run away orthogonally. Besides, the modification in the shock strength at the trailing edge will induce a change in the wake development downstream of the cascade, qualitatively similar to what we described for the ideal-like scenario but to a larger quantitative extent. Lower but still significant variations also affect the reflected shock and the fish-tail flow pattern that arise from the suction side, revealing a flow field highly altered by operational uncertainty.

Furthermore, a peculiar evolution of the Mach number uncertainty can be observed in the blade channel of the non-ideal cascade. A zero variation is calculated at the throat, where a sonic Mach number ($M = 1$) always onsets. Then, Mach number values are affected by a large uncertainty, which cannot be prompted by area-ratio variation alone. The inspection of the Mach number distribution against the pressure in Fig. 9, obtained with the quasi-one-dimensional approach detailed §2, can elucidate on this matter. Negligible variations are found in Fig. 9(a) for the ideal-like case, consistently with the $CoV(M)$ field in Fig. 8(a). As for the non-ideal expansion, a non-monotonic trend of the Mach number against the pressure is predicted in Fig. 9(b), in accordance with the corresponding flow field in Fig. 4. In this context, the local minimum and maximum are strongly altered by operational uncertainty, thus justifying the high-uncertain region within the blade channel detected in the Mach number field but absent in the pressure field.

As a final comment, we note that operational uncertainty largely perturbs cascade nominal operation within a non-ideal framework, presumably affecting the overall cycle performance as well. The combination of quasi-one-dimensional analyses with stochastic analyses sheds light on the physical nature of these variations, which are found to be mainly related to the high sensitivity of the A/A^* on the upstream total temperature. Alongside the large performance deviations in the supersonic stator, operational uncertainty induces a highly uncer-

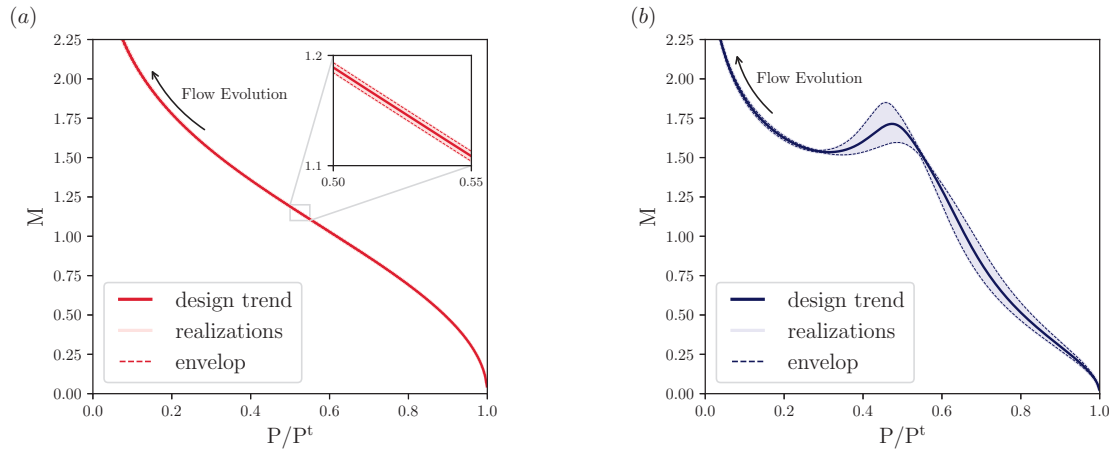

Figure 9: Design Mach number distributions predicted by the quasi-one-dimensional theory for an ideal-like expanding flow (with total states $P^t = 8\,\text{bar}$ and $T^t = 272.5\,^\circ\text{C}$) and a non-ideal expanding flow (with total states $P^t = 40\,\text{bar}$ and $T^t = 272.5\,^\circ\text{C}$) of fluid MM, along with 200 independent uniformly distributed realizations assuming $\pm 1.25\%$ uncertainty in both the design total pressure and temperature.

tain flow delivered to the first rotating-blade row, which may further amplify the overall efficiency variation of the turbine. The estimate of this additional non-ideal implication will be the core of the next section.

5. Consequences on the rotor aerodynamics

The previous analysis showed that the first rotating cascade has to operate with a highly variable incoming flow when the stator expansion process occurs in the non-ideal regime ($\Gamma \ll 1$). Although the rotor experiences higher values of Γ (e.g in the present case, the minimum value is $\Gamma = 0.5 - 0.6$ at the inlet, becoming $\Gamma = 0.9 - 1.0$ as long as the expansion proceeds), a variation in the incoming flow might still provoke a departure from its nominal conditions. Two main issues may arise: (i) a variation in the relative Mach number field, inducing supersonic flow regime at the rotor inlet and, consequentially, unique-incidence operation [42]; (ii) a variation in the flow angle, yielding a positive or negative incidence at the rotor leading edge, thus affecting both the work extracted and the stage reaction degree and efficiency.

As for the first point, the inspection of Mach number uncertainty in Fig. 8 reveals that only the wake (low Mach number region) is altered by operational uncertainty, while the free-stream Mach number is practically constant. In fact, variations occurring in the ideal-like nozzle cascade are not enough large to have a perceivable effects on the value of the free-stream Mach number. For the non-ideal cascade, the operational uncertainty does entail large variations, but operation in the neighbourhood of a stationary point (i.e. the local minimum) makes the Mach number robust to perturbations in the pressure field (e.g. given by modifications in the shock strength). Moreover, the non-monotonic trend of the Mach number in Fig. 9 shows that the sensitivity of the Mach number on

the upstream total state attenuate getting closer to the local minimum.

On the contrary, variations in the incidence angle will require a deeper investigation, as many thermodynamic variables are involved in a complex way. To do so, some preliminary considerations on the rotating cascade are needed. As design criteria, we assume that $\alpha_2 = 0°$, where the subscript 2 refers to the rotor outlet section. It means that the flow leaving the rotor is completely axial, thus minimising the outlet kinetic energy. A straightforward manipulation of the rothalpy balance ($h + (w^2 - u^2)/2 =$ const. across the rotor, where w and u are the relative and peripheral velocity, respectively) combined with the velocity-triangle relationship ($\mathbf{v} = \mathbf{u} + \mathbf{w}$, where the bold font indicates vectors), and assuming $v_0^2 \ll v_1^2$ ($v_0^2/v_1^2 < 0.05$ for both supersonic stators), yields the following equation:

$$\frac{u}{v_1} = \frac{\chi}{2(1-\chi)\sin\alpha_1} + \frac{\sin\alpha_1}{2}, \qquad (4)$$

Plugging into Eq. (4) the pitchwise mass-flow averages of v_1 and α_1 that are extracted from the nominal flow fields at half axial chord downstream of the trailing edge $x/c_{ax} = 1.50$ (as plausible stator-rotor gap), we estimated the peripheral speed for the two cases. Next, prescribing zero incidence at design conditions, we determine the rotor-inlet blade angle for the ideal-like and non-ideal case. In Fig. 10, rotor incidence distributions i_{rot} downstream of the stator trailing edge are reported. It is clear that the average value of zero-incidence at nominal conditions is obtained by balancing the negative peaks (provided by the wake) with the positive peaks (provided by shock waves). Nonetheless, large pitchwise deviations of incidence

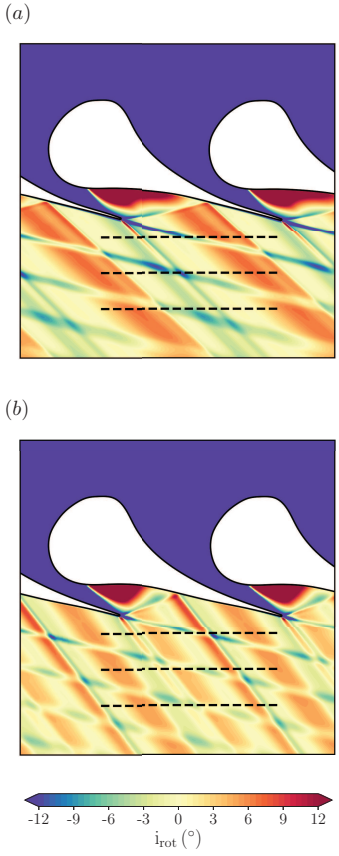

Figure 10: Rotor incidence angle downstream of the ideal-like (b) and non-ideal (b) stator cascade. The black dashed lines indicate three axial traverses at $x/c_{ax} = 1.15, 1.45, 1.75$, where pitchwise distributions are extracted.

from the average value might substantially increase the stator-rotor interaction, with a further burden on the overall stage performance [43].

These incidence fluctuations are related to the non-uniform flow field delivered by the first-stator cascades; as previously discussed, in strongly non-ideal conditions this flow field is highly affected by operational uncertainty. In this context, two points need to be addressed: first, quantifying the corresponding uncertainty on the rotor incidence, thus assessing whether the rotor departs from nominal conditions; second, establishing an optimal stator-

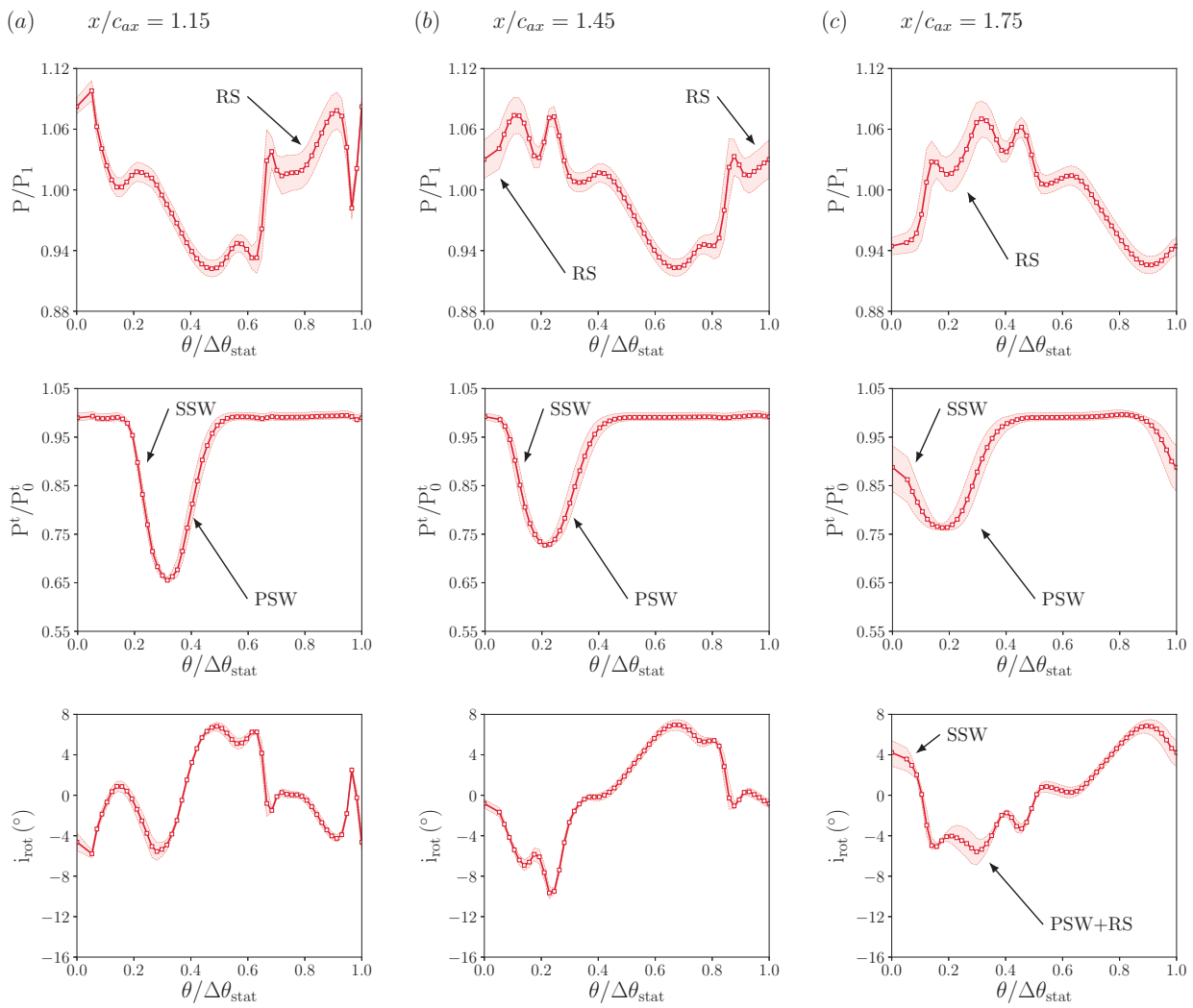

Figure 11: Pitchwise distributions of pressure, total pressure and rotor incidence angle at different axial transverse downstream of the stator trailing edge for the ideal-like cascade. The nomenclature of the uncertainties is reported in Fig. 8.

rotor gap (if any) such that the superposition of the two competitive effects (wake and shocks) reduces the overall incidence variations. For illustrative purposes, pitchwise distributions of pressure, total pressure and incidence are reported in Fig. 11 and Fig. 12 for the ideal-like and non-ideal case, respectively, at three selected downstream axial traverses, namely $x/c_{ax} = 1.15, 1.45, 1.75$. Pressure distributions enable to visualise the modification in shock strength, while total-pressure distributions highlight the evolution of the wake under uncertainty. From these trends it is possible to better appreciate the relationship between the stochastic fields, described in the previous section, with the corresponding physical values. The same designations previously devised are here adopted to outline the uncertainty peaks in the corresponding distributions.

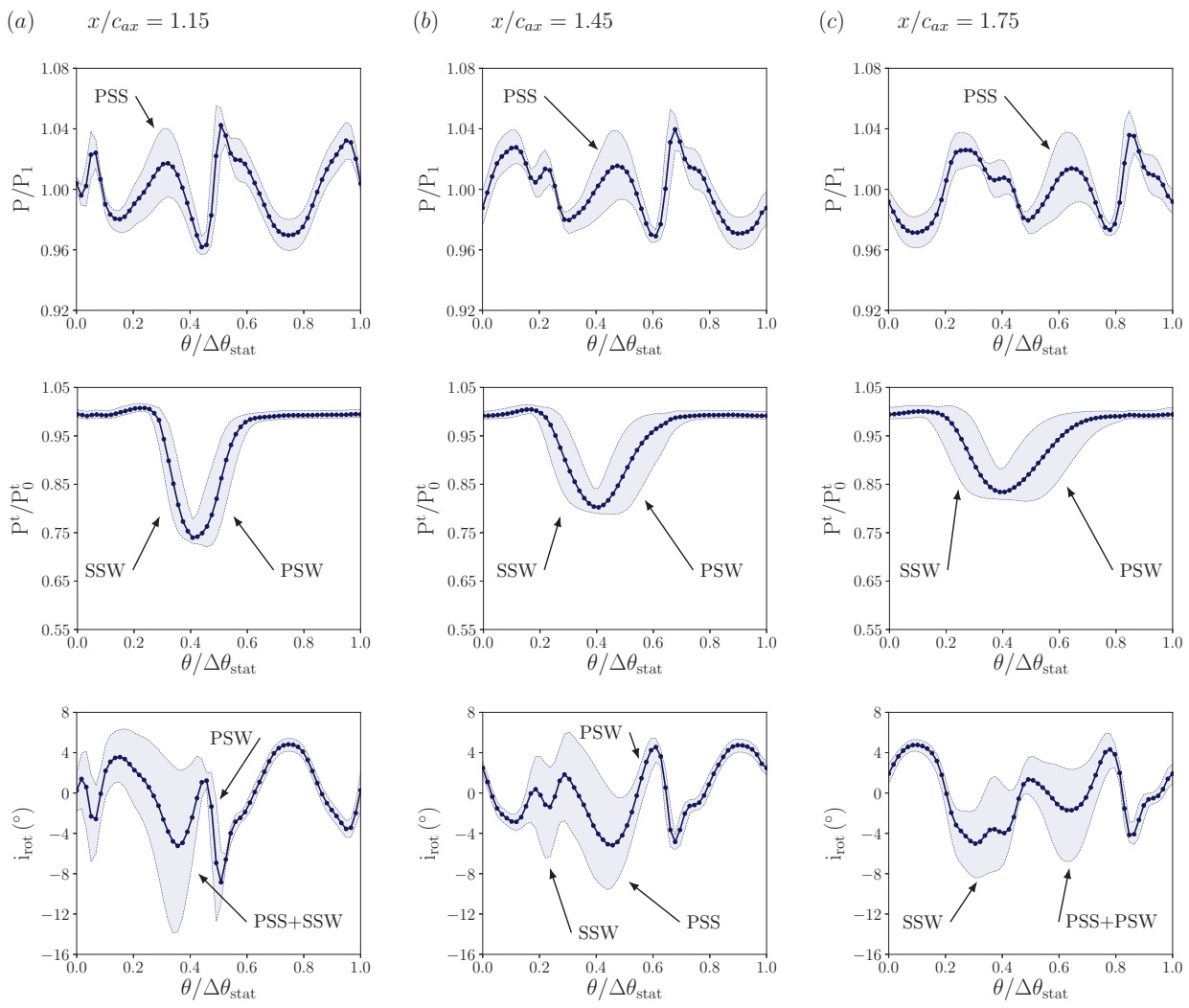

Figure 12: Pitchwise distributions of pressure, total pressure and rotor incidence angle at different axial transverse downstream of the stator trailing edge for the non-ideal cascade. The nomenclature of the uncertainties is reported in Fig. 8.

In the ideal-like scenario, the main uncertainty is the pressure value behind the reflected shock. While the shock is smeared moving to downstream as a consequence of the mixing process, the induced uncertainty just slightly changes. On the other hand, the uncertainty in the wake morphology, both in terms of width and depth, is almost negligible for the ideal-like case. A noticeable variation is only found in the distribution at $x/c_{ax} = 1.75$, as shown in the central frame of Fig. 11(c). In this case, there is an amplification of the wake uncertainty when the reflected shock intercepts the wake coming from the suction side. Moreover, the shock-induced uncertainty in the pressure field seemingly rises the corresponding uncertainty in the pressure-side branch of the wake. Connected to this uncertainty combination that arises from the shock-wake interactions, the incidence distribution becomes lo-

cally uncertain as well, notwithstanding the small extent of such variations in terms of both the region and magnitude. For the other cases, in which the shock-induced uncertainty runs into the free stream, see Fig. 11(a)-(b), variations in the incidence nominal trend can be barely recognised.

A more complex situation is depicted by the non-ideal scenario in Fig. 12. Consistently with the stator analysis, uncertainties are overall more significant. From pressure trends, it can be noticed that the main variation is right before the reflected shock, opposed to the ideal-like case; as explained above, this uncertainty arises from the shock modification at the blade opening, propagating downstream orthogonally to the shock front. Pressure trends at different measurement planes are nearly identical, while the wake evolution in the total-pressure fields shows that its uncertainty increases as long as the mixing process occurs. The combination of these effects directly impacts on the determination of the incidence uncertainty. At $x/c_{ax} = 1.15$, the uncertainty that is induced by the pressure-side shock (PSS) couples with the uncertainty in the suction-side branch of the wake (SSW); the superposition of these two uncertainties yields a sharp incidence drop ($i_{rot} - i_{rot,des} = -10°$). While moving downstream, the main pressure uncertainty progressively intercepts the pressure-side branch of the wake and its associated uncertainty (PSW). Differently from the previous case, the superposition of these two effects does not produce an appreciable increase in the incidence uncertainty. As a matter of fact, only PSS and SSW seem to affect the incidence trend, while PSW only provides a negligible contribution.

The evident alteration of the pitchwise incidence distribution under operational uncertainty confirms that a non-ideal gas-dynamic regime in the supersonic stator may also trigger off-design operation in the subsequent rotor cascade. As a further proof of that, Fig. 13 reports the pitchwise-averaged incidence angle $\overline{i_{rot}}$ at different axial transverse downstream of the stator cascade. The averaged incidence varies $\pm 0.3°$ and $\pm 3.0°$ as a consequence of an ideal-like and non-ideal gas dynamics, respectively. The quantitative impact of such variations on the rotor aerodynamics will depend on the specific 3D blade design, operating conditions and flow regime. As a general guideline, we suggest applying design criteria that make the rotor more robust against incidence variations, e.g. privileging a rotor design with a larger leading-edge radius. Moreover, there seems not to be an advantageous axial location where the rotor can be conveniently placed without incurring in such large incidence variations. Therefore, the classical criteria for determining the stator-rotor axial gap also apply in the non-ideal scenario.

6. Discussion on cycle implications

The significant performance departures that affect first-stage supersonic turbines when $\Gamma \ll 1$ are expected to promote variations in the cycle nominal conditions in several ways. Following the previous discussions, stator and rotor aerodynamic losses are largely sensitive to operational uncertainty, as a consequence of shock-pattern and incidence-angle modifications, respectively. The two effects couple in the determination of the first-stage and, hence,

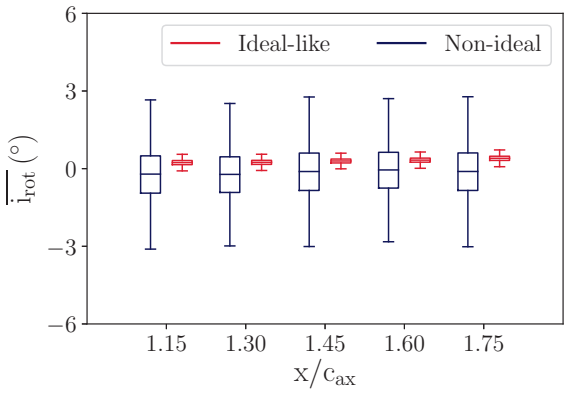

Figure 13: Evolution of the pitchwise-averaged rotor incidence angle along the axial coordinate for the ideal-like and non-ideal cascade.

turbine isentropic efficiency η_T. Many studies advocate that the ORC plant efficiency considerably depends on the turbine-efficiency value [7, 44], thus allowing us to qualitatively link the observed turbine variations to as many variations in the cycle efficiency.

The turbine efficiency also enters into the power output, via the relationship $\dot{W} = \dot{m}\,\Delta h_{is}\,\eta_T - \dot{W}_p - \dot{W}_{aux}$, where Δh_{is} is the isentropic enthalpy drop associated with the turbine expansion, and $\dot{W}_p$ and $\dot{W}_{aux}$ are the powers consumed by the pump and auxiliaries, respectively. Moreover, significant variations in the mass flow rate characterise the non-ideal scenario, as reported in §4 (up to ±4% with respect to the design value). Nonetheless, a negative correlation between the mass flow rate and the isentropic enthalpy drop is found in those thermodynamic conditions. It follows that the product $\dot{m}\,\Delta h_{is}$ changes less compared to the mass-flow-rate variation alone. $\dot{W}_p$ and $\dot{W}_{aux}$ depends on the mass-flow rate as well, but the corresponding contributions to the overall power is expected to be of second order with respect to turbine-induced variations.

A change in the mass flow rate may also trigger off-design operation in the heat exchangers, affecting both heat-transfer coefficients and thermal powers. To cite an example, preliminary off-design analyses of the transcritical cycle, accounting directly for the observed mass-flow-rate variations, show that the pinch-point temperature at the regenerator can change up to ±2.5 °C.

Most of the variations in the non-ideal regime are associated with the high sensitivity of the expansion process to the upstream turbine total temperature, i.e. the maximum temperature of the cycle. Although the system dynamics may hinder some of these effects, a careful control of the maximum temperature becomes mandatory to ensure proper plant operation at nominal conditions.

Finally, we stress that the results here discussed only include small perturbations of the nominal conditions, which can be conveniently treated as independent random variables. Off-design operation features a larger variability in the boundary conditions [45], which cannot in principle be considered purely stochastic because ORC systems follow precise control strategies. In this context, departures from the nominal conditions are expected to be even more significant than the ones previously reported, with a consequent deterioration of the cycle part-load performance. A quantitative example is reported in Romei *et al.* [22], where an increase of 20 °C in the upstream total temperature tripled the aerodynamic losses of a supersonic cascade that expanded in highly non-ideal conditions. These evidences highlight the crucial role of the first nozzle-

cascade aerodynamics in the overall cycle performance when the associated expansion process takes place in the non-ideal gas-dynamic regime. Further studies that include such non-conventional turbine behaviour within cycle design and analysis are therefore compulsory for future high-temperature transcritical ORCs.

7. Generalisation to other organic fluids

Until now, the analysis was limited to specific thermodynamic conditions of MM expanding flows. In this section, we aim at generalising our findings to a wider class of organic fluids. The amplification of operational uncertainty was mainly due to the significant sensitivity of throat thermodynamic properties with respect to the upstream total state. We showed that a variation in the throat thermodynamic conditions, namely in the density and speed of sound, has a paramount importance both in the mass flow rate processed by the (choked) cascade and in its aerodynamic losses, as a consequence of A/A^* modification. Specifically, the variation in the nominal trend of A/A^* is recognised as the main contributor to the change in the cascade performance. Based on this physical backbone, the A/A^* trend can be conveniently used to predict whether non-ideal gas-dynamic regimes amplify small departures from nominal conditions.

To this end, Fig. 14 reports area-ratio evolutions against the pressure, along with Γ and Z fields, for three expanding flows of exemplary fluids, namely a refrigerant (R1234yf, $C_3H_2F_4$), an aromatic hydrocarbon (Toluene, C_7H_8) and a linear siloxane (MDM, $C_8H_{24}O_2Si_3$). The choice of these fluids is motivated by their comparatively different molecular complexity, which is closely linked with the achievable minimum Γ [17]. Different fluids that belong to the same class (refrigerants, hydrocarbons, siloxanes) are expected to share comparable values of Γ close to the critical point, thus behaving similarly from a non-ideal gas-dynamic perspective. The reduced total temperatures for the three expansions are $T^t/T_C = 1.13, 1.08, 1.04$, respectively. The reduced total pressure is $P^t/P_C = 2$ for all expansions. The total states are selected to achieve very low values of Γ and Z along the expansions, while avoiding two-phase flows when uncertainties are included. To be consistent with the methodology applied in §2, a variation of $\pm 1.25\%$ in both total quantities (with temperature measured in Celsius degrees) is here considered. Within this framework, 200 independent realisations are reported in Fig. 14 along with the A/A^* nominal trend.

The inspection of the area-ratio evolution (bottom panels) reveals that the amplification of the operational uncertainty increases with the molecular complexity. Similar tests performed with other fluids (consisting in linear, cyclic and aromatic hydrocarbons, refrigerants, and linear and cyclic siloxanes) seemingly confirm this conjecture. As previously noted, the thermodynamic parameters contributing mostly to performance variations were the density and the speed of sound at the throat and their associated gradients. The departure of both density and speed of sound from the ideal-gas behaviour is accounted in either Z or Γ, hence one might question whether one of these two parameters can better describe the sensitivity of the expansion process with respect to the upstream total

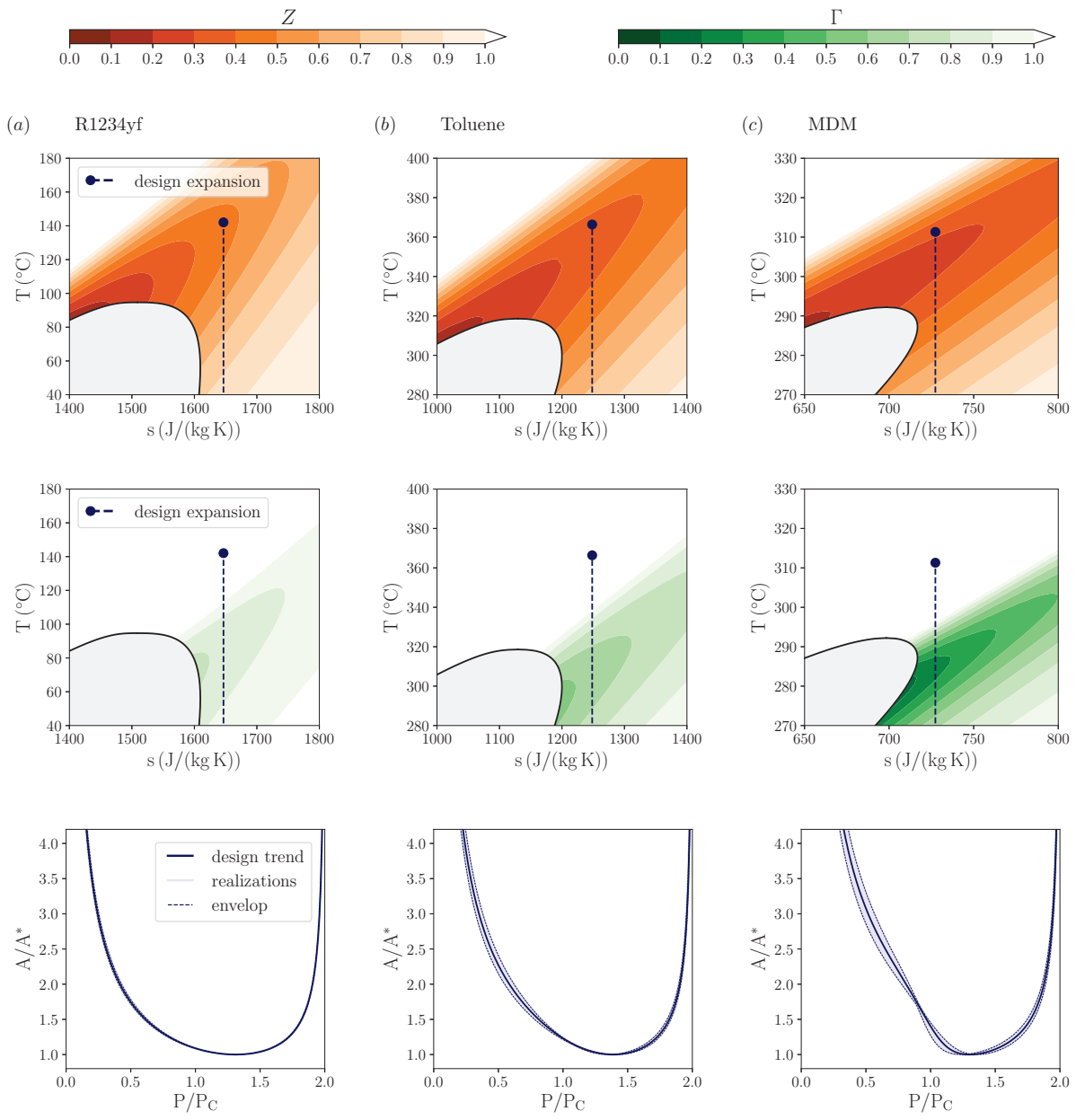

Figure 14: Design area-ratio distributions (bottom frames) predicted by the quasi-one-dimensional theory for (a) the refrigerant R1234yf (with total states $P^t/P_C = 2$ and $T^t/T_C = 1.13$), (b) the aromatic hydrocarbon Toluene (with total states $P^t/P_C = 2$ and $T^t/T_C = 1.08$) and (c) the linear siloxane MDM (with total states $P^t/P_C = 2$ and $T^t/T_C = 1.03$), along with 200 independent uniformly distributed realizations assuming $\pm 1.25\%$ uncertainty in both the design total pressure and temperature (measured in Celsius degree). Maps of the compressibility factor Z (top frames) and fundamental derivative of gas dynamics Γ (central frames) are superposed to the design expansion process in the temperature–specific entropy plane.

conditions. It is worth to underline that neither Γ nor Z can be linked to a single property variation (irrespective of whether density or speed of sound) without altering the other from the ideal-

gas behaviour. From Fig. 14, Γ, which is strictly related to the molecular complexity of the fluid, seems to discriminate the quantitative variations in A/A^* and, implicitly, in the cascade performance, notwithstanding low values of Γ and Z share a large portion of the thermodynamic region in molecularly complex fluids. As a matter of fact, all expansion processes feature very low values of Z, i.e. $Z_{min} = 0.47, 0.34, 0.27$ along the isentropic expansions of R1234yf, toluene and MDM, respectively, but comparatively different levels of Γ, whose minimum values are $\Gamma_{min} = 0.82, 0.63, 0.27$, respectively. Moreover, it seems that variations triggered by non-ideal flows are quantitatively limited up to $\Gamma_{min} \approx 0.8$, while becoming progressively more significant for lower values of Γ.

To conclude, in addition to qualitative non-ideal effects that exclusively depend on Γ, e.g. the non-monotonic trend of the Mach number against the pressure or the increase of the Mach number across an oblique compression shock, also quantitative departures from the nominal trend, mostly given by the dependency of the expansion process on the upstream total state, seem to be mainly linked to Γ. Following the results of this analysis, when dealing with molecularly complex fluids we suggest to inspect the Γ evolution along the isentropic expansion and the corresponding sensitivity of A/A^* with respect to the upstream total variables to be aware of the potential larger variability triggered by non-ideal operation.

8. Conclusion and final recommendations

This paper discussed the implications of the non-ideal gas-dynamic regime on the cascade, turbine and cycle performance. To this end, a probabilistic framework that accounts for small operational uncertainty was formulated, combining an uncertainty-quantification strategy based on polynomial-chaos representations with Reynolds-averaged Navier-Stokes flow simulations. The computational framework is applied to first-stage supersonic cascades, operating both in ideal-like $\Gamma \gtrsim 0.8$ and non-ideal $\Gamma \lesssim 0.8$ conditions.

Numerical results highlighted the large sensitivity of cascade performance on the upstream total state, in particular on the upstream total temperature, in presence of non-ideal flows. The mass flow rate and the cascade losses were found to change four and six times more than their ideal-like counterpart, respectively, given the same relative variations in the boundary conditions. The physical reasons behind these variations were illustrated by means of the general steady isentropic quasi-one-dimensional flow theory. It was shown that a change in the upstream total temperature largely affects the density and the speed of sound at the throat, therefore: (i) the mass flow rate directly changed as a consequence of turbine choked operation, (ii) the area-ratio A/A^* evolution changed along the expansion, thus triggering off-design operation. As a matter of fact, a variation in A/A^* will impose a different adapted pressure ratio across the cascade, which has to rely on modification of the shock-pattern at the trailing edge to fulfil the prescribed expansion process with a consequent al-

teration of nominal losses.

On top of that, the entire flow field in non-ideal conditions was found to be highly affected by operational uncertainty. As a result, the subsequent rotor cascade has to deal with a variable incoming flow. As such, the rotor incidence angle changed both locally (up to 10 °) and in average (±3 °), opposed to nearly null variations in the ideal-like scenario.

Furthermore, non-ideal flows through the nozzle cascades are also expected to influence other cycle components; for example, a variation in the mass flow rate can induce off-design operation in heat exchangers, altering both heat-transfer coefficients and thermal powers.

Finally, the qualitative agreement with the general steady flow theory enabled the generalisation of present findings to other molecularly complex fluids. Furthermore, preliminary numerical evidences arguably suggested that Γ can be conveniently used to predict such variations, allowing the cycle designer to anticipate potential pitfalls associated with the non-ideal gas-dynamic regime.

References

[1] M. Astolfi, M. C. Romano, P. Bombarda, E. Macchi, Binary ORC (organic Rankine cycles) power plants for the exploitation of mediumlow temperature geothermal sources Part A: Thermodynamic optimization, Energy 66 (2014) 423 – 434. doi:10.1016/j.energy.2013.11.056.

[2] J. Freeman, K. Hellgardt, C. N. Markides, An assessment of solar-powered organic rankine cycle systems for combined heating and power in uk domestic applications, Applied Energy 138 (2015) 605 – 620. doi:10.1016/j.apenergy.2014.10.035.

[3] A. M. Pantaleo, S. M. Camporeale, A. Miliozzi, V. Russo, N. Shah, C. N. Markides, Novel hybrid csp-biomass chp for flexible generation: Thermo-economic analysis and profitability assessment, Applied Energy 204 (2017) 994 – 1006. doi:10.1016/j.apenergy.2017.05.019.

[4] H. Yu, X. Feng, Y. Wang, L. T. Biegler, J. Eason, A systematic method to customize an efficient organic Rankine cycle (ORC) to recover waste heat in refineries, Applied Energy 179 (2016) 302 – 315. doi:10.1016/j.apenergy.2016.06.093.

[5] A. Schuster, S. Karellas, R. Aumann, Efficiency optimization potential in supercritical organic rankine cycles, Energy 35 (2) (2010) 1033 – 1039. doi:10.1016/j.energy.2009.06.019.

[6] N. A. Lai, M. Wendland, J. Fischer, Working fluids for high-temperature organic Rankine cycles, Energy 36 (1) (2011) 199 – 211. doi:10.1016/j.energy.2010.10.051.

[7] P. Colonna, E. Casati, C. Trapp, T. Mathijssen, J. Larjola, T. Turunen-Saaresti, A. Uusitalo, Organic Rankine Cycle power systems: From the concept to current technology, applications, and an outlook to the future, J. Eng. Gas Turb. Power 137 (10) (2015) 100801–1–19.

[8] E. Macchi, M. Astolfi, 9 - Axial flow turbines for Organic Rankine Cycle applications, in: E. Macchi, M. Astolfi (Eds.), Organic Rankine Cycle (ORC) Power Systems, Woodhead Publishing, 2017, pp. 299 – 319. doi:10.1016/B978-0-08-100510-1.00009-0.

[9] A. Meroni, J. G. Andreasen, G. Persico, F. Haglind, Optimization of organic Rankine cycle power systems considering multistage axial turbine design, Applied Energy 209 (2018) 339 – 354. doi:10.1016/j.apenergy.2017.09.068.

[10] A. P. S. Wheeler, J. Ong, The role of dense gas dynamics on organic rankine cycle turbine performance, J. Eng Gas Turb. Power 135 (10) (2013) 102603.

[11] E. Rinaldi, R. Pecnik, P. Colonna, Unsteady operation of a highly supersonic orc turbine, Journal of Turbomachinery 128 (12) (2016) 121010.

[12] M. Pini, G. Persico, D. Pasquale, S. Rebay, Adjoint method for shape optimization in real-gas flow applications, Journal of Engineering for Gas Turbines and Power 137 (2015) 1–13.

[13] G. Persico, P. Rodriguez-Fernandez, A. Romei, High-fidelity shape-optimization of non-conventional turbo-

machinery by surrogate evolutionary strategies, Journal of Turbomachinery 141 (8) (2019) 081010.

[14] P. A. Thompson, A fundamental derivative in gasdynamics, Phys. Fluids 14 (9) (1971) 1843–1849.

[15] P. A. Thompson, K. C. Lambrakis, Negative shock waves, J. Fluid Mech. 60 (1973) 187–208.

[16] M. S. Cramer, Negative nonlinearity in selected fluorocarbons, Phys. Fluids A 1 (11) (1989) 1894–1897.

[17] P. Colonna, A. Guardone, Molecular interpretation of nonclassical gasdynamics of dense vapors under the van der Waals model, Phys. Fluids 18 (5) (2006) 056101–1–14.

[18] N. R. Nannan, A. Guardone, P. Colonna, On the fundamental derivative of gas dynamics in the vapor–liquid critical region of single-component typical fluids, Fluid Phase Equilib. 337 (2013) 259–273.

[19] M. S. Cramer, L. M. Best, Steady, isentropic flows of dense gases, Phys. Fluids A 3 (4) (1991) 219–226.

[20] D. Vimercati, G. Gori, A. Guardone, Non-ideal oblique shock waves, J. Fluid Mech. 847 (2018) 266–285.

[21] A. Spinelli, G. Cammi, S. Gallarini, M. Zocca, F. Cozzi, P. Gaetani, V. Dossena, A. Guardone, Experimental evidence of non-ideal compressible effects in expanding flow of a high molecular complexity vapor, Exp. fluids 59 (2019) 1–16. doi:10.1007/s00348-018-2578-0.

[22] A. Romei, D. Vimercati, G. Persico, A. Guardone, Non-ideal compressible flows in supersonic turbine cascades, Journal of Fluid Mechanics 882 (2020) A12. doi:10.1017/jfm.2019.796.

[23] E. A. Bufi, P. Cinnella, X. Merle, Sensitivity of Supersonic ORC Turbine Injector Designs to Fluctuating Operating Conditions, ASME Turbo Expo: Turbomachinery Technical Conference and Exposition V02BT39A012 (GT2015-42193) (2015) 1–15.

[24] N. Razaaly, G. Persico, P. M. Congedo, Impact of geometric, operational, and model uncertainties on the non-ideal flow through a supersonic ORC turbine cascade, Energy 169 (2019) 213 – 227. doi:10.1016/j.energy.2018.11.100.

[25] P. A. Thompson, Compressilbe Fluid Dynamics, McGraw-Hill, 1988.

[26] M. Thol, F. H. Dubberke, G. Rutkai, T. Windmann, A. Köster, R. Span, J. Vrabec, Fundamental equation of state correlation for hexamethyldisiloxane based on experimental and molecular simulation data, Fluid Phase Equilibria 418 (2016) 133 – 151. doi:10.1016/j.fluid.2015.09.047.

[27] P. Colonna, J. Harinck, S. Rebay, A. Guardone, Real-gas effects in organic rankine cycle turbine nozzles, J. Propul. Power 24 (2) (2008) 282–294.

[28] M. Preissinger, D. Bruggemann, Thermal Stability of Hexamethyldisiloxane (MM) for High-Temperature Organic Rankine Cycle (ORC), Energies 9 (3). doi:10.3390/en9030183.

[29] L. Keulen, S. Gallarini, C. Landolina, A. Spinelli, P. Iora, C. Invernizzi, L. Lietti, A. Guardone, Thermal stability of hexamethyldisiloxane and octamethyltrisiloxane, Energy 165 (2018) 868 – 876. doi:10.1016/j.energy.2018.08.057.

[30] G. Persico, M. Pini, 8 - Fluid dynamic design of Organic Rankine Cycle turbines, in: E. Macchi, M. Astolfi (Eds.), Organic Rankine Cycle (ORC) Power Systems, Woodhead Publishing, 2017, pp. 253 – 297.

[31] R. Bini, D. Colombo, Large multistage axial turbines, Energy Procedia 129 (2017) 1078 – 1084. doi:10.1016/j.egypro.2017.09.138.

[32] F. J. D. Galiana, A. P. S. Wheeler, J. Ong, A study of trailing-edge losses in Organic Rankine Cycle turbines, J. Turbomach. 138 (12) (2016) 121003.

[33] F. J. D. Galiana, A. P. S. Wheeler, J. Ong, C. A. de M Ventura, The effect of dense gas dynamics on loss in ORC transonic turbines, Journal of Physics: Conference Series 821 (1) (2017) 012021.

[34] L. Zanellato, M. Astolfi, A. Serafino, D. Rizzi, E. Macchi, Field performance evaluation of geothermal ORC power plants with a focus on radial outflow turbines, Renewable Energydoi:10.1016/j.renene.2018.08.068.

[35] A. Romei, D. Vimercati, A. Guardone, G. Persico, The role of operational variability on the non-ideal flow in supersonic turbines for supercritical organic Rankine cycles, in: Proceedings of the 5th International Seminar on ORC Power Systems, The National Technical University of Athens (NTUA), 2019, pp. 184: 1–9.

[36] E. W. Lemmon, M. L. Huber, M. O. McLinden, NIST reference database 23: reference fluid thermodynamic

and transport properties–REFPROP, version 9.1, Standard Reference Data Program.

[37] O. Le Maître, O. M. Knio, Spectral Methods for Uncertainty Quantification: With Applications to Computational Fluid Dynamics, Scientific Computation, Springer Netherlands, 2012.

[38] B. K. Askey, J. Wilson, Some Basic Hypergeometric Orthogonal Polynomials that Generalize Jacobi Polynomials, American Mathematical Society, 1985.

[39] T. Crestaux, O. Le Maître, J. M. Martinez, Polynomial chaos expansion for sensitivity analysis, Reliability Engineering and System Safety 94 (7) (2009) 1161 – 1172. doi:10.1016/j.ress.2008.10.008.

[40] D. J. Mee, N. C. Baines, M. L. G. Oldfield, T. E. Dickens, An Examination of the Contributions to Loss on a Transonic Turbine Blade in Cascade, Journal of Turbomachinery 114 (1) (1992) 155–162. doi:10.1115/1.2927979.

[41] J. D. Denton, L. Xu, The trailing edge loss of transonic turbine blades, J. Turbomach. 112 (2) (1990) 277–285.

[42] E. A. Bufi, P. Cinnella, Preliminary design method for dense-gas supersonic axial turbine stages, Journal of Engineering for Gas Turbines and Power 140 (11) (2018) 112605.

[43] P. Gaetani, G. Persico, C. Osnaghi, Effects of axial gap on the vane-rotor interaction in a low aspect ratio turbine stage, Journal of Propulsion and Power 26 (2) (2010) 325–334. doi:10.2514/1.37616.

[44] E. Macchi, 1 - Theoretical basis of the Organic Rankine Cycle, in: E. Macchi, M. Astolfi (Eds.), Organic Rankine Cycle (ORC) Power Systems, Woodhead Publishing, 2017, pp. 3 – 24. doi:10.1016/B978-0-08-100510-1.00001-6.

[45] R. Dickes, O. Dumont, L. Guillaume, S. Quoilin, V. Lemort, Charge-sensitive modelling of organic Rankine cycle power systems for off-design performance simulation, Applied Energy 212 (2018) 1262 – 1281. doi:https://doi.org/10.1016/j.apenergy.2018.01.004.